

IMAGING LARGE SCALE STRUCTURE IN THE X-RAY SKY

Y. YANG^{1,2}, R. F. MUSHOTZKY², A. J. BARGER^{3,4,5}, L. L. COWIE⁵, D. B. SANDERS^{5,6}, A. T. STEFFEN³

Submitted to the Astrophysical Journal Letters

ABSTRACT

We present the first results from a wide solid angle, moderately deep *Chandra* survey of the Lockman Hole North-West region. Our 9 ACIS-I fields cover an effective solid angle of 0.4 deg² and reach a depth of 3×10^{-16} erg cm⁻² s⁻¹ in the 0.4–2 keV band and 3×10^{-15} erg cm⁻² s⁻¹ in the 2–8 keV band. The best fit logN-logS for the entire field, the largest contiguous *Chandra* field yet observed, matches well onto that of the *Chandra* Deep Field North. We show that the full range of the ‘cosmic variance’ previously seen in different *Chandra* fields is reproduced in this small region of the sky. Counts-in-cells analysis shows that the hard band sources are more strongly correlated than the soft band sources.

Subject headings: cosmology: observations — large-scale structure of the universe — x-rays: diffuse background—galaxies: nuclei

1. INTRODUCTION

Recent *Chandra* and *XMM* observations have resolved over 85% of the 2–8 keV X-ray background (XRB) into discrete sources, presumably active galactic nuclei (AGNs; Mushotzky et al. 2000; Brandt et al. 2001; Tozzi et al. 2001; Campana et al. 2001; Cowie et al. 2002; Giacconi et al. 2002; Hasinger et al. 2001). However, the nature of the sources is unclear, with many of the faint sources showing little or no optical activity (Barger et al. 2001, 2002; Hornschemeier et al. 2001; Rosati et al. 2002). There is a large field-to-field variance in the source counts in the *Chandra* deep surveys in the 2–8 keV band (Cowie et al. 2002). This cosmic variance is generally believed to arise from the underlying large-scale structure (LSS) that is traced, in some fashion, by the *Chandra* sources. Clustering of the XRB sources in redshift space has been seen in both *Chandra* Deep Fields (Barger et al. 2002; Hasinger 2002), indicating that LSS does exist in the XRB source distribution. From a cosmological point of view, AGNs are expected to be highly biased tracers of cosmic structure formation at medium to large redshifts. The XRB sources, which have ~ 10 times the areal density of optically selected AGNs, provide for the first time a sufficiently high density to be used as tracers of the LSS.

The clustering at various scales of X-ray selected AGNs has been pursued previously using observations from *HEAO-1* (e.g. Barcons & Fabian 1988; Mushotzky & Jahoda 1992) and *ROSAT* (e.g. Soltan et al. 1997; Vihkinlin & Forman 1995). The *ROSAT* results based on deep pointings (Carrera et al. 1998) show a much smaller amplitude of correlation than predicted from optical samples, while an analysis of the *ROSAT* North Ecliptic Pole sample, which is shallower but covers a wider solid angle (Mullis 2002), comes to the opposite conclusion. It has been claimed that at a flux level below 1.5×10^{-15} erg cm⁻² s⁻¹ (0.5–2 keV) the XRB exhibits no clustering

(Soltan & Hasinger 1994). This contradicts the observed cosmic variance in the ultradeep surveys by *Chandra* and *XMM*. How to combine these seemingly disparate results is one of the new mysteries of the XRB.

To allow a direct measurement of the auto-correlation functions (ACFs) of the XRB sources, and to optically identify these objects to obtain their redshifts, one needs arcsecond spatial resolution, a wide contiguous field of view, and sufficient sensitivity. To achieve these goals we have performed a large solid angle, moderately deep *Chandra* survey of the Lockman Hole North-West region. This survey currently has a contiguous sky coverage of ~ 0.4 deg² and is sensitive to X-ray flux levels of 3×10^{-16} erg cm⁻² s⁻¹ (0.4–2 keV) and 3×10^{-15} erg cm⁻² s⁻¹ (2–8 keV). Most of the XRB is resolved at these flux levels (Cowie et al. 2002).

2. OBSERVATIONS AND DATA REDUCTION

The survey covers the Lockman Hole North-West region centered at $\alpha = 10^h 34^m$, $\delta = 57^\circ 40'$ (J2000). The region has very low Galactic column density ($N_H \equiv 5.72 \times 10^{19}$ cm⁻², Dickey & Lockman 1990) and was covered by the deepest 170 μ m ISOPHOT field observed from *ISO* (hereafter ISONW). The field has also been observed at 850 μ m with the SCUBA camera on the James Clerk Maxwell Telescope and at cm wavelengths with the VLA, as well as at optical and near-IR wavelengths with the Subaru (using the unique Suprime-Cam instrument) and Keck telescopes. The ISONW region will be intensively observed with *SIRTF* as part of the LEGACY program. The multiwavelength analysis of this field will be presented in subsequent papers.

The observation consists of 9 ACIS-I pointings (labeled as ISONW1–ISONW9) separated from each other by $\sim 10'$ to allow close to uniform sky coverage. ISONW1 has an exposure time of ~ 70 ks while the other 8 pointings have

¹ Department of Astronomy, University of Maryland, College Park 20742-2421

² Laboratory for High Energy Astrophysics, Goddard Space Flight Center, Code 660, NASA, Greenbelt, MD, 20770

³ Department of Astronomy, University of Wisconsin at Madison, 5534 Sterling Hall, 475, Madison, WI 53760

⁴ Department of Physics and Astronomy, University of Hawaii, 2505 Correa Road, Honolulu, HI 96822

⁵ Institute for Astronomy, University of Hawaii, 2680 Woodlawn drive, Honolulu, HI 96822

⁶ Max-Planck-Institut für Extraterrestrische Physik, D-85740, Garching, Germany

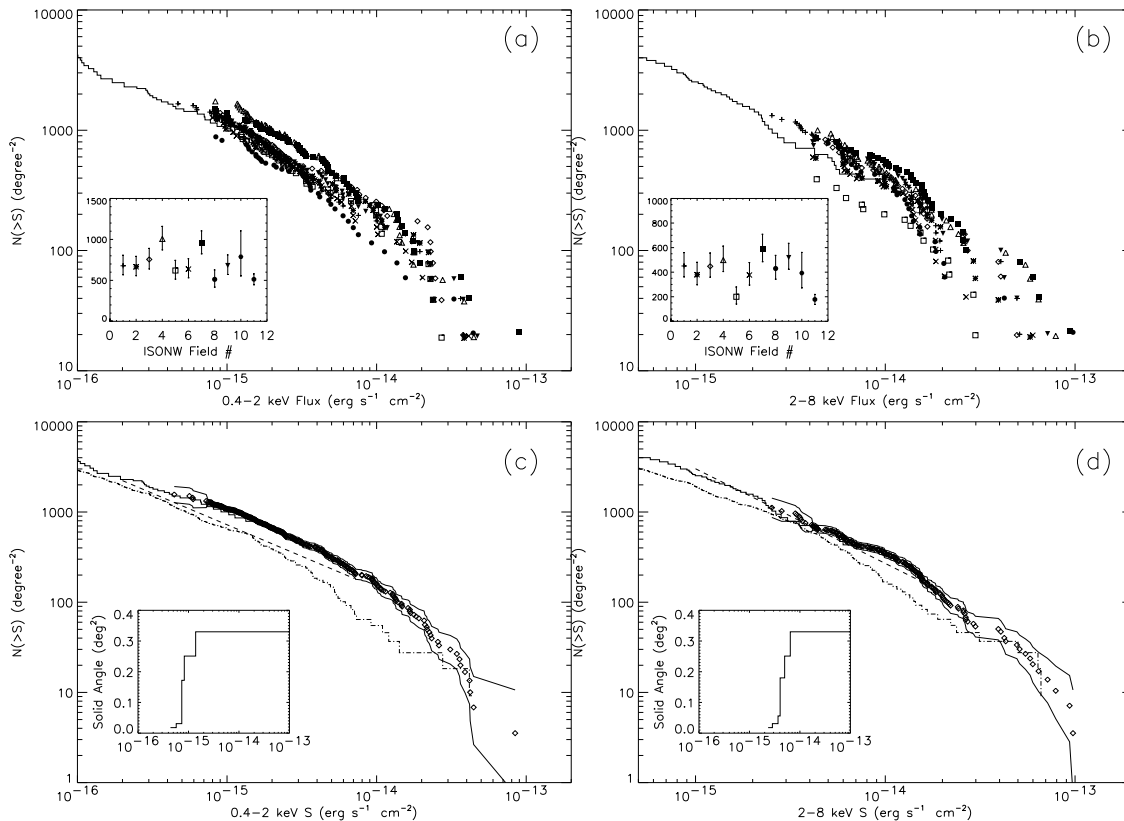


FIG. 1.— The cumulative number counts in the 9 fields (a), (b) and the whole field (c), (d). For each (a) and (b), the insert shows the number counts of each ISONW field at flux level of 2×10^{-15} erg cm $^{-2}$ s $^{-1}$ (soft) and 9×10^{-15} erg cm $^{-2}$ s $^{-1}$ (hard). The solid line is the logN-logS of CDF-N. Field numbers 10 and 11 represents the CDF-N and CDF-S value respectively. The highest counts in the 9 fields are about 2.3 (soft) and 3.3 (hard) times higher than that from CDF-S, which has the lowest normalization among all the deep surveys (Cowie et al. 2002). For the hard band, number counts of 8 of the 9 fields are $\sim 1\sigma$ about the mean, but ISONW5 is much lower. For each (c) and (d), cumulative number counts for the whole field (diamonds with solid lines representing the Poisson error) is compared with that from CDF-N (solid histogram), CDF-S (dash-dotted histogram) and SSA13 (dashed line). The inserts shows the sensitive sky area vs flux.

exposure times of ~ 40 ks.

The data were reduced with CIAO 2.2.1 and CALDB 2.15. The CXC *Science Threads* were followed in data preparation. The resulting event lists were binned into 2 energy bands, the soft (0.4–2 keV) and the hard (2–8 keV).

Point sources were detected for each pointing in both energy bands with *wavdetect* within the CIAO package. The wavelet scales of square root series 1, $\sqrt{2}$, 2, $2\sqrt{2}$, 4, $4\sqrt{2}$, 8 and a false detection threshold of 1×10^{-7} were used. Spectrally weighted monochromatic exposure maps were created, assuming a power law with photon index of 1.2 for the hard band and 1.4 for the soft band (Mushotzky et al. 2000; Barger et al. 2001). Count rates were converted to flux assuming the above power law spectra with only Galactic absorption. The conversion factors are 4.74×10^{-12} erg cm $^{-2}$ (soft) and 2.34×10^{-11} erg cm $^{-2}$ (hard). The degradation of the ACIS low energy quantum efficiency during the flight was corrected using the measurements of the ACIS team.

The catalogs for all observations were merged. Source properties for objects detected in more than one observation (due to the overlapping of fields) were taken from the field in which the source had the smallest off-axis angle. In the soft band, 431 sources were detected, and in the hard band, 278. The combined catalog contains 554 sources.

3. ANALYSIS AND RESULTS

Since the effective area decreases and the point spread function (PSF) increases with off-axis angle, the sensitivity is not uniform across the field. We quantified this with Monte-Carlo simulations. First we constructed background maps by removing the wavelet detected sources from the observed images and filled the holes with Poisson noise sampled from regions surrounding the sources. Sources with fluxes drawn from the LogN-LogS derived from the *Chandra* deep fields (Cowie et al. 2002; Garmire 2002) were generated and distributed uniformly within $8'$ from the aim point. PSF images of each source were made using *mkpsf*. The exposure maps described in the previous section were then applied to simulate the effect of vignetting. The simulated sources were added to the background maps to create simulated images. About 100 simulations were performed for each band and exposure (for details see Yang et al. 2003). Above flux thresholds of 10 cts/exposure (soft) and 12 cts/exposure (hard), the detection is complete and the derived fluxes are consistent with the input values. We use the flux unit in cts/exposure because we found the *wavdetect* exposure-corrected count rates threshold in such unit only depends weakly on the exposure time in our observations due to the low backgrounds. We obtain the same results by assuming a uniform background and the *wavdetect* detection thresholds described in Freeman et al. (2002). Within $4.5'$ of the aim

point, the detection is complete above 5 cts/exposure in the soft band and 7 cts/exposure in the hard band.

Above flux thresholds of 1.2×10^{-15} erg cm $^{-2}$ s $^{-1}$ (soft) and 8×10^{-15} erg cm $^{-2}$ s $^{-1}$ (hard), the source catalog in the combined field within 8' from each aim point is complete. This defines a flux limited sample that contains 115 hard band and 298 soft band sources. The solid angle covered by the complete sample field is 0.33 deg 2 .

We constructed the cumulative number counts (LogN-LogS) for each of 9 fields, as well as the whole merged catalog (Fig. 1). The Eddington bias found at these flux levels from the simulations is small and can be ignored.

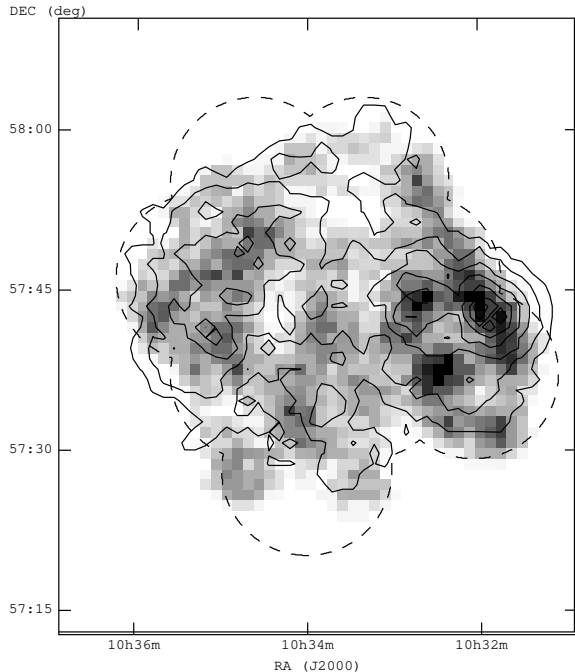


FIG. 2.— The density map of the flux limited samples (region outlined with a dashed line). The maps have been adaptively smoothed using *fadapt* in *FTOOLS* with a 6 counts kernel counts threshold. The gray scale map represents the source density in the soft band. The contours show the source density in the hard band. The 7 contour levels are proportional to the logarithm of the source density.

Fig. 1a and 1b show comparisons of the LogN-LogS in the 9 pointings. Although the overlapping of fields could minimize the differences between them, this is the simplest way to demonstrate the cosmic variance because exactly the same procedures were used in each field and 8 of the 9 fields have virtually identical exposures. Variance is seen in both the soft and hard bands. The full range of variance seen in the *Chandra* deep surveys published to date is reproduced in this set of contiguous fields.

The LogN-LogS of the whole field is compared with that from *Chandra* deep field North (CDF-N; Brandt et al 2001), the *Chandra* Deep Field south (CDF-S, Rosati et al. 2001) and SSA13 (Mushotzky et al. 2000) in Fig. 1c and 1d. Our LogN-LogS connects smoothly with that of CDF-N, which has the highest normalization of all the published *Chandra* deep fields.

The LogN-LogS distribution of the combined fields is modeled with power laws in the form of $N(> S) = A(S/S_0)^{-\alpha}$, using the area weighted maximum likelihood method (Murdoch, Crawford & Jauncey 1973). For the soft band, between 2×10^{-15} and 10^{-14} erg cm $^{-2}$ s $^{-1}$, $A =$

630, $S_0 = 2 \times 10^{-15}$, and $\alpha = 0.72 \pm 0.18$; above 1×10^{-14} erg cm $^{-2}$ s $^{-1}$, $A = 152$, $S_0 = 1 \times 10^{-14}$, and $\alpha = 1.58 \pm 0.23$. For the hard band above 1×10^{-14} erg cm $^{-2}$ s $^{-1}$, the best fit parameters are $A = 359$, $S_0 = 1 \times 10^{-14}$, and $\alpha = 1.56 \pm 0.16$.

To visualize the source distributions, we used adaptive smoothing to create density maps of the flux limited sample (Fig.2). Structure is visible in both the soft and hard band maps, but the hard band sources are more clustered. To test whether the observed over-density could arise from Poisson fluctuations, we employed the likelihood test described in Carrera et al.(1998). Comparing with 10000 simulated samples which are Poisson distributed, we found 97.67% of the soft and 99.99% of the hard band simulations had better likelihood than the observations. The significance of clustering is therefore 2σ (soft) and 4σ (hard).

Using the source distribution in cells tiling the field (counts-in-cells), we can estimate the correlation scales of the sources. The variance of counts-in-cells defined as $\mu_2 \equiv \langle (N - \bar{N})^2 \rangle$, where \bar{N} is the mean counts in the cell, is directly related to the angular correlation function (Peebles 1980) by

$$\mu_2 = \bar{N} + \frac{\bar{N}^2}{\Omega^2} \int w(\theta) d\Omega_1 d\Omega_2 \quad (1)$$

where Ω is the cell size. The first term is the Poisson fluctuation. For correlation functions with a power-law form $w(\theta) = (\theta/\theta_0)^{1-\gamma}$ (where γ is the power law index of the spatial correlation function) and square cells with size $\Omega = \Theta \times \Theta$ deg 2 , the integration can be obtained as (Totsuji & Kihara 1969; Lahav & Saslaw, 1992),

$$\sigma^2 \equiv \frac{\mu_2 - \bar{N}}{(\bar{N}/\Omega)^2} = C_\gamma \theta_0^{1-\gamma} \Theta^{5-\gamma} \quad (2)$$

where σ^2 is the normalized variance. C_γ is a function of γ and is calculated numerically. We calculate σ^2 for square cells of various sizes that tile the whole field. By fitting the $\sigma^2 - \Theta$ relation we should be able to estimate θ_0 and γ . We found the present data cannot constrain both parameters accurately. By fixing $\gamma = 1.8$, the ‘universal’ slope measured in galaxies and in groups and clusters of galaxies (Bahcall 1988), and minimizing χ^2 , we found $\theta_0 = 40 \pm 11''$ and $\theta_0 = 4 \pm 2''$ for the hard and soft band sources respectively. While the soft band sources agree very well with the angular correlation scale previously seen in *ROSAT* surveys (Vikhlinin & Forman, 1995), the hard band sources are much more strongly correlated.

The striking difference in clustering between the soft and hard band sources indicates the hard sources which are not detected in the soft band are highly clustered. About 60% of the hard-band-only sources lie in overdense regions which form a ‘band’ connecting the ‘lumps’ on the western and eastern side of the field (Fig. 2). This band includes only about 1/3 of solid angle of the whole field. The counts-in-cells analysis (Fig. 3) also indicates that these hard-band-only sources have larger correlation scales than the soft band or hard band sources.

4. DISCUSSION

ASCA observations have shown that the rms variance of the 2–10 keV XRB on a scale of 0.5 deg 2 is $\sim 6\%$ (Kushino et al. 2002). With a sky coverage of 0.4 deg 2 and a depth

that resolves $> 50\%$ of the hard band XRB, the normalization of LogN-LogS derived from our observations should be very close to the “true” value. The fact that the observed LogN-logS connects onto the CDF-N field at low fluxes then indicates that $> 90\%$ of the XRB is resolved using the *ASCA/ROSAT* XRB normalization (Chen et al. 1997). The main uncertainty is the normalization of XRB itself.

The LSS seen in our field has reproduced the cosmic variance observed previously in deep field surveys. It is noticeable (Fig. 1b) that on scales of a *Chandra* field the variance is demonstrated as holes rather than lumps, i.e., the number counts in 9 fields are close to the mean, while only 2 fields have very low value (ISONW5 & CDF-S). This indicates the existence of voids in the X-ray LSS, which should, within a factor of a few, be of the same angular size as an ACIS-I field. Most of the hard-band-only sources cluster in relatively small regions, which may be topologically connected. If this is not a result of a projection effect, then it is the first time a wall-like structure has been seen in the X-ray sky.

We have found more variance in the hard band than in the soft band, consistent with the lower mean redshift of the hard X-ray sources. However, the difference in the mean redshift cannot account for most of the large difference in the soft and hard band angular correlation length found by the counts-in-cells statistic. The mean redshift found previously for the *Chandra/XMM* deep fields sources is ~ 0.8 . Unless most of the hard band sources are at very low redshift, which does not seem likely because we see no low redshift spikes in the redshift distribution of deep field surveys, the relatively low redshifts for the hard X-ray selected sources could not account for the factor of 10 larger differences in correlation scales seen in these sources. The similarity of the redshift distributions for the sources found in CDF-N and in an observation with a similar exposure to ours (Castander et al. 2003), indicates that the luminosity functions have likely been sampled below the “knee” for all redshifts in our observations. Thus we feel that the stronger correlation function for the hard sources seen in our data is likely due to their stronger spatial correlation rather than a redshift effect.

The large variance in the *Chandra* source counts indi-

cates that they must be highly biased tracers of matter. Direct calculation of the bias will require redshifts and an understanding of how the luminosity function changes with redshift, but it is already clear that the *Chandra* sources show much more variance than galaxy counts (Cohen et al 2000) at similar optical magnitudes.

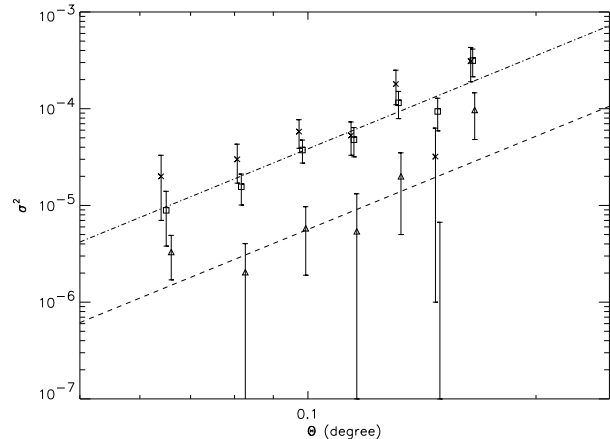


FIG. 3.— Normalized variance σ^2 measured with different sized square cells which tiles the whole field. Squares: the hard band sources; triangles: the soft band sources. Crosses: the hard band only sources. The errors are estimated via a boots-trap technique. The lines shows the best fit variance with $\gamma = 1.8$ (fixed) and $\theta_0 = 40'' \pm 11$ for the hard band, $\theta_0 = 4'' \pm 2$ for the soft band sources. The hard-band-only points are not fitted due to the small number of sources.

We thank CXC for their excellent work, G. Garmire and N. Brandt for providing the CDF-N logN-logS, C. Reynolds, K. Arnold, K. Jahoda, D. Davis, K. Kuntz, D. Smith and A. Young for very helpful discussions. The project is funded under IDS program of R. Mushotzky, NSF grants AST-0084847 (A.J.B.) and AST-0084816 (L. L. C.), the University of Wisconsin Research Committee with funds granted by the Wisconsin Alumni Research Foundation (A.J.B.) and the Alfred P. Sloan Foundation (A.J.B.). D. B. S. gratefully acknowledges the hospitality of the MPE and is grateful for support from a senior award from the Alexander von Humboldt-Stiftung and from NASA through Chandra Award number GO2-3191C.

REFERENCES

- Bahcall, N. A., 1988 ARA&A, 26, 631
 Barcons, X. & Fabian, A. C. 1988, MNRAS, 230, 189
 Barger, A. J., Cowie, L. L., Mushotzky, R. F., Richards, E. A. 2001 AJ,121,662
 Barger, A. J., Cowie, L. L., Brandt, W. N., Capak, P., Garmire, G. P., Hornschemeier, A. E., Steffen, A. T., Wehner, E. H. 2002, AJ, 124, 1839
 Brandt, W. N., Alexander, D. M., Hornschemeier, A. E., Garmire, G. P., Schneider, D. P., Barger, A. J., Bauer, F. E., Broos, P. S. et al. 2001 AJ, 122, 2810
 Campana, S., Moretti, A., Lazzati, D., Tagliaferri, G. 2001, ApJ, 560, L19
 Carrera, F. J., Barcons, X., Fabian, A. C., Hasinger, G., Mason, K. O., McMahon, R. G., Mittaz, J. P. D., Page, M. J. 1998, MNRAS299, 229
 Castander, F. J., Treister, E., Maza,Z., Coppi,P., Maccarone, T., Zepf, Z., Guzman, R., Ruiz, M. T. 2003, Proceedings of the "X-ray surveys, in the light of the new observatories" workshop, Astron. Nachr., in press
 Cohen, J. G., Hogg, D. W., Blandford, R., Cowie, L. L., Hu, E., Songaila, A., Shopbell, P., Richberg, K. et al. 2000, ApJ, 538, 2
 Cowie, L. L., Garmire, G. P., Bautz, M. W., Barger, A. J., Brandt, W. N., Hornschemeier, A. E. 2002, ApJ, 566, L5
 Chen, L.-W.; Fabian, A. C.; Gendreau, K. C. 1997 MNRAS, 285, 449
 Dickey & Lockman, 1990, ARA&A, 28, 215
 Freeman, P. E., Kashyap, V., Rosner, R., Lamb, D. Q. 2002, ApJS, 138, 185
 Garmire, 2002, private communication
 Giacconi, R., Zirm, A., Wang, J., Rosati, P., Nonino, M., Tozzi, P., Gilli, R., Mainieri, V. et al. 2002, ApJS, 139, 369
 Hasinger, G., Altieri, B., Arnaud, M., Barcons, X., Bergeron, J., Brunner, H., Dadina, M., Dennerl, K. et al. 2001, A&A, 365, L51
 Hasinger, G. 2002, AAS Conference 199 No.138.19
 Hornschemeier, A. E., Brandt, W. N., Garmire, G. P., Schneider, D. P., Barger, A. J., Broos, P. S., Cowie, L. L., Townsley, L. K. et al. 2001 ApJ554, 742
 Kushino, A., Ishisaki, Y., Morita, U., Yamasaki, N. Y., Ishida, M., Ohashi, T., Ueda, Y. 2002, PASJ, 54, 327
 Lahav, O., Saslaw, W. C. 1992, ApJ, 396, 430L
 Mullis, C. R., 2002, PASP 114,688
 Murdoch, H. S., Crawford, D. F., Jauncey, D. L. 1973, ApJ, 183, 1
 Mushotzky, R. F., Cowie, L. L., Barger, A. J., Arnaud, K. A., 2000, Nature, 404, 459

- Mushotzky, R. & Jahoda, K., 1992, in *The X-ray Background*, eds. Barcons, X., Fabian, A. C., Cambridge University Press, Cambridge
- Peebles, P. J. E., 1980, *The Large Scale Structure of the Universe*, Princeton University Press
- Rosati, P., Tozzi, P., Giacconi, R., Gilli, R., Hasinger, G., Kewley, L., Mainieri, V., Nonino, M. et al. 2002, ApJ, 566, 667
- Soltan, A. & Hasinger, G. 1994, A&A, 288, 77
- Soltan, A. M., Hasinger, G., Egger, R., Snowden, S., Truemper, J. 1997, A&A, 320, 705
- Totsuji, H., Kihara, T. 1969, PASP, 21, 221
- Tozzi, P., Rosati, P., Nonino, M., Bergeron, J., Borgani, S., Gilli, R., Gilmozzi, R., Hasinger, G. et al. 2001, ApJ, 562, 42
- Vikhlinin, A., Forman, W. 1995, ApJ, 455, L109